A MIM/Coaxial Stub-Line CRLH Zeroth-Order Series-Mode Resonator used as an RF Coil Element for 7-Tesla Magnetic Resonance Imaging

Andreas Rennings[1], Jan Taro Svejda[1], Simon Otto[2], Klaus Solbach[2], and Daniel Erni[1]

[1]General and Theoretical Electrical Engineering (ATE), [2]High Frequency Engineering (HFT), Faculty of Engineering, University of Duisburg-Essen, and [1]CENIDE – Center for Nanointegration Duisburg Essen, D-47048 Duisburg, Germany

Abstract—A novel MIM/coaxial-stub composite right/left-handed (CRLH) metamaterial transmission-line (TL) structure is proposed. In addition to the common metal-insulator-metal (MIM) series capacitor, a short-circuited coaxial line, which is vertically aligned to the otherwise planar structure, forms the shunt inductor. The zeroth-order (ZO) series mode with its spatially uniform and longitudinally polarized series current of the short-circuited CRLH TL is utilized in the context of RF field excitation in a 7-Tesla magnetic resonance imaging (MRI) scanner. The usage of coaxial stubs instead of sidewise microstrip lines has several advantages, especially for the MRI application, such as a unit cell with smaller width, the unwanted longitudinal magnetic field components excited by the shunt resonantor are shielded by the outer coaxial connector and the upper MIM plate, yielding a high Q_{sh}-to-Q_{se}-ratio (here 250/100), which implies an extremely uniform series current distribution. Here a 40-cm long ZO resonant element for 300 MHz is proposed. FEM eigen-mode and FDTD driven-mode full-wave simulation, together with corresponding near-field measurements on fabricated prototypes are presented to comfirm the approach.

Index Terms—*CRLH metamaterial transmission-line; zeroth-order resonator (ZOR); MRI RF coil*

I. INTRODUCTION

The zeroth-order resonance (ZOR) phenomenon of a CRLH metamaterial line [1] can be utilized, e.g., for electrically short (miniaturization) or electrically long (high directivity) antennas [2], due to the excellent scalability of the ZO resonator, just by changing the number of CRLH unit cells. Additionally to these far-field devices, the spatially constant field distribution along a periodic ZO resonator is also an attractive property for a near-field device, like the RF coil of a magnetic resonance imaging (MRI) scanner. For the MRI application a transversally polarized RF[1] magnetic field denoted with B_1 is desired, which is orthogonal to the longitudinally polarized DC magnetic field denoted by B_0 (longitudinal direction = bore axis) [3]. The magnitude of B_1 must be as constant as possible in the so-called field-of-view (FOV[2]), which is always located in the human body. The longitudinally uniform magnitude is an inherent ZOR property [1]. It has been firstly exploited for the MRI application in [4]. Later publications use the same CRLH cell topology with MIM-capacitors and sidewise microstrip-line (MSL) based stubs [5], [6]. In [6] the first multi-channel coil based on eight ZOR elements was presented for head imaging at 9.4 Tesla.

---

[1]The oscillation frequency f_{RF} of the B_1 field is proportional to B_0, the DC magnetic field. f_{RF} is usually located in the VHF range.
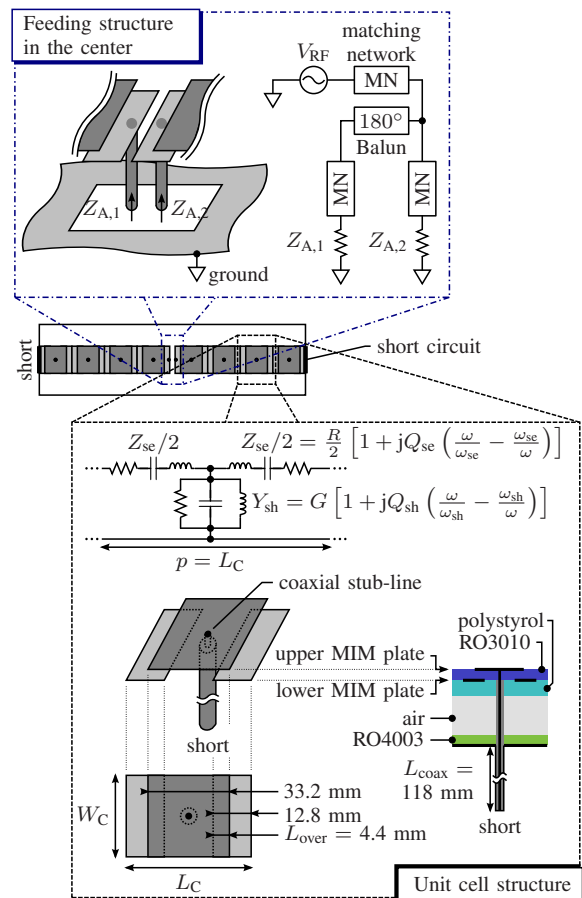
[2]The FOV can be a plane or a volume.

Fig. 1. Proposed 8-cell RF coil element together with a zoomed view of one unit cell with the novel MIM/coaxial stub-line topology, and another zoomed view onto the backside feeding network including a $180°$ balun and 3 matching networks with high-voltage trim capacitors (not shown) allowing a balanced fed. Perspective, top and lateral view onto one unit cell, where the later indicates the stack-up including a 0.25 mm-thick RO3010 substrate for the MIM capacitors, a 1.0 mm-thick polystyrol layer for mechanical support, 5 mm of air, and a RO4003 substrate with a thickness of 0.5 mm for the backside ground-plane.

Here a novel CRLH cell topology is proposed, which is optimized for the MRI application in terms of near-field performance and geometry (minimal transversal width, maximal longitudinal length). Compared to earlier ZO series mode antennas, a balanced feeding technique is used. The longitudinally symmetric resonator is more robust with respect to sheath waves on the feeding line, an important feature for the

MRI application. The topology of the novel CRLH structure and the corresponding ZOR RF coil element is introduced in Sec. II. Detailed full-wave results based on FEM eigen-mode simulation with COMSOL and FDTD driven-mode simulations with EMPIRE XCcel, together with measurements of fabricated prototypes, are given in Sec. III.

II. MIM/COAXIAL STUB-LINE CRLH RESONATOR

Basically the sidewise MSL stubs of older CRLH unit cells [1], [2], [4] are replaced by coaxial-line versions. As depicted in Fig. 1 the inner conductor of the coax line is connected to the upper MIM plate, whereas its outer conductor is soldered to the back-side ground plane. In this case the shunt resonator is shielded from the volume above the element, where the human body will be located, thus a high Q_{sh} can be expected. The ZOR element is fed symmetrically by using a balun, since the initial version presented in [4], which is fed at one end of the short-circuited CRLH TL, is prone to sheath waves on the feeding cable. The balanced feeding scheme is depicted in the upper right of Fig. 1.

III. FULL-WAVE SIMULATION & MEASUREMENT RESULTS

The design of the RF coil element is a three-step procedure. Due to the periodicity of the CRLH metamaterial structure an eigen-mode based simulation technique – here with FEM/COMSOL – where only one unit cell is considered and periodic boundaries are applied (cf. Fig. 2(a)), can be used to efficiently tune the operation frequency f_{RF}, to meet the so-called frequency-balanced condition [1] ($f_{se} = f_{sh} = f_{RF}$) and to maximize the Q_{sh}-to-Q_{se}-ratio, which will lead to the desired spatially constant series current.
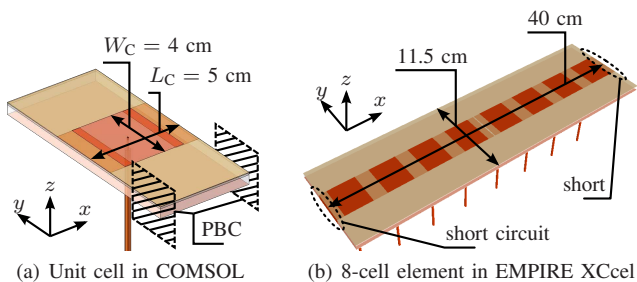

Fig. 2.   Models for the eigen- and driven-mode simulations.

After this initial eigen-mode simulation a driven-mode based simulation technique – here with FDTD/EMPIRE XCcel – is carried out, in order to study the effects of the finite length of the CRLH structure (cf. Fig. 2(b)) and the feeding position, which is located at the center of the eigth-unit-cell RF element, where a small gap (1.4 mm) is introduced (cf. Fig. 1). With the help of EMPIRE XCcel the excited EM fields – usually the magnetic field amplitude $|\vec{H}|$ and the local specific absorption rate (SAR), which is proportional to $|\vec{E}|^2$ – are investigated. At this intermediate FDTD-based simulation step a fine-tuning of the geometry is commonly sufficient.

For both simulation types a flat phantom with the material parameters $\varepsilon_r = 45.3$ and $\sigma = 0.87$ S/m has been utilized to consider the influence of the human body at 300 MHz. The phantom has a thickness of 25 cm and is 5 cm separated from the upper MIM plate of the structure, which corresponds to the plane at $z = 0$ cm.

During the third and final step the trimmer capacitors are determined via a circuit based simulation technique – here with ADS – where the input impedances of the intrinsic RF coil element are considered via a Touchtone file obtained from the FDTD simulation or alternatively from measurements.

A. Eigen-mode Simulation with COMSOL (FEM)

Based on the efficient one-unit-cell-only eigen-mode simulation the influence of several geometrical parameters on the resonance frequency and Q-factor of the two involved resonators are investigated. For this purpose a vanishing phase-shift along the unit cell is used. Due to lack of space, here only the results of two geometrical parameters, the length of the coaxial stub-line, L_{coax}, and the overlap of the upper and lower MIM plates, L_{over}, are given. Both parameters have only influence on one resonance frequency, f_{sh} or f_{se}. The corresponding plots are given in Fig. 3. With this knowlegde an initially frequency-unbalanced design can be easily tuned to the desired frequency-balanced case.
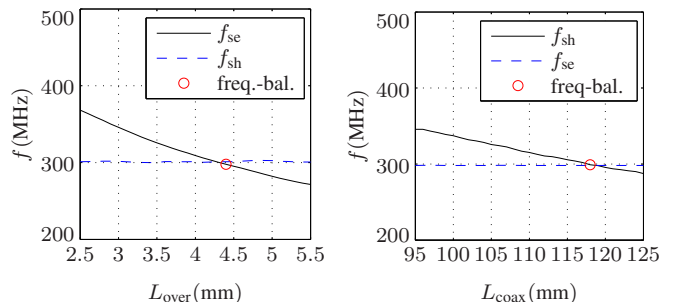

Fig. 3.   Influence of the parameters L_{over} and L_{coax} on the resonance frequencies f_{se} and f_{sh}. Results are obtained by FEM eigen-mode simulation for $\phi = 0°$.

The dispersion diagram (for small phase shifts between the two PBCs in x-direction) together with the corresponding Q-factors for a frequency-balanced unit cell design with $f_{se} = f_{sh} = 300$ MHz has been calculated and is shown in Fig. 4.

The behavior of the two resonance frequencies for different phase shift along the unit cell is well established [1], [2], whereas the dependency of the two Q-factors is still under investigation [7]. For our ZOR based application a zero phase shift along the cell is impressed within the eigen-mode simulation. In this case the series- and the shunt-resonator of the equivalent circuit is decoupled[3] and the Q_{sh}-to-Q_{se}-ratio is therefore maximized. Here an excellent Q-factor-ratio of $250/100 = 2.5$ has been simulated. The higher this ratio the smaller the series current decay away from the central feeding point (cf. Fig. 1). Compared to older CRLH cells

---

[3]The decoupling at zero phase shift occurs only for a transversally symmetric unit cell, yielding the same Bloch impedance for a forward- and backward traveling wave [8].
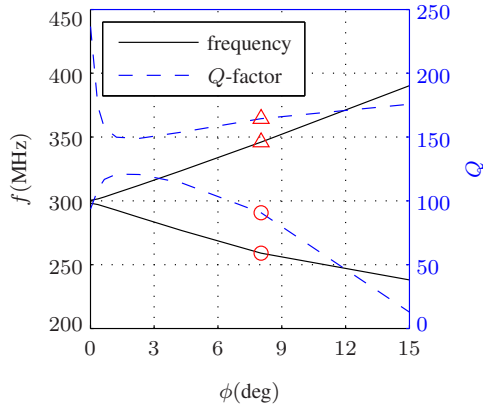
Fig. 4. Dispersion diagram together with the corresponding Q-factors for a frequency-balanced design with $f_{sh} = f_{se} = 300$ MHz.

with open[4] stub-lines [1], [2], the new closed coaxial stub-lines yield higher values for Q_{sh} and therefore a better series current homogeneity.

For a non-zero phase shift along the unit cell the series and shunt resonators are no longer decoupled. Therefore the Q-factors are "averaged" and their ratio is reduced as depicted in Fig. 4. For a phase shift of around $2°$ the Q-factor-ratio reaches a minimum of $150/120 \approx 1.25$. For further increased phase shift the Q-factor of the right-handed mode [1] (the corresponding curves in Fig. 4 are marked with $\triangle$) is slightly increased, whereas the Q-factor of the left-handed mode [1] (the corresponding curves in Fig. 4 are marked with $\circ$) is strongly decreased. We may conclude that the non-ideal left-handed elements (series capacitor and shunt inductor) exhibit higher losses than their right-handed counterparts (series inductor and shunt capacitor).

B. Driven-mode Simulation with EMPIRE XCcel (FDTD)

The FDTD-simulated EM fields excited by the RF coil element are given as surface plots in Fig. 5. The plot of the electrical current density inside the upper MIM plate, $\vec{J}(x, y, z = 0$ cm$)$, in Fig. 5(a) indicates two aspects, the vector-field is purely longitudinally polarized, and its magnitude is spatially constant along that direction (x). The plot for the excited magnetic field 2 cm inside the phantom, $\vec{H}(x, y, z = 7$ cm$)$, is displayed above. The plot reveals again a purely polarized magnetic vector field with no longitudinal component, and a corresponding magnitude with a maximum directly opposite to the feeding position and a decay away from that. The $|\vec{H}(x, y, z = 7$ cm$)|$ distribution is smoother than the exciting one, $|\vec{J}(x, y, z = 0$ cm$)|$, due to the "low-pass property" of the space, which extents from the upper MIM plate at $z = 0$ cm to the evaluation plane inside the flat phantom at $z = 7$ cm. The same is true for the SAR distribution with is even smoother due to the involved square operator (SAR $\propto |\vec{E}|^2$).

[4]The term "open" refers here to non-shielded or open-to-free-space. Thus a higher radiation resissitance must be expected, yielding a lower Q-factor.

(a) current density in upper MIM plate & magnetic field 2 cm inside flat phantom

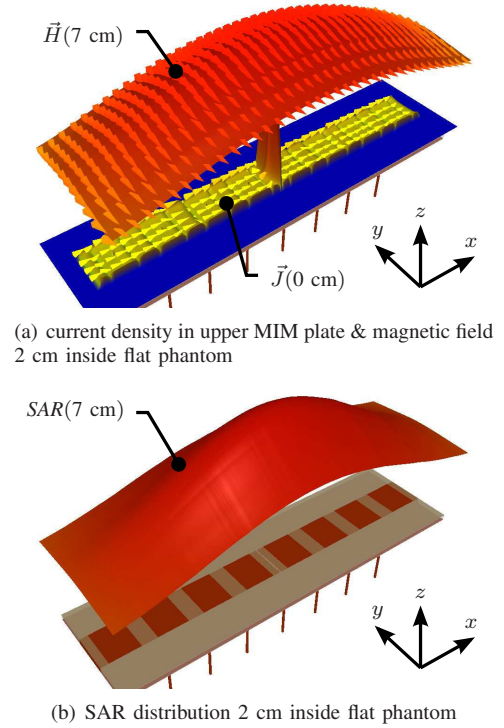(b) SAR distribution 2 cm inside flat phantom

Fig. 5. FDTD simulated fields of the 8-cell MIM/coax-stub CRLH element.

C. Prototypes and Near-field Measurements

The front- and back-side of an eight-cell MIM/coax-stubs prototype is shown in Fig. 6. For comparison an older prototype with meandered sidewise stubs, which has a larger transversal dimension[5], is given as well (upper part of the figure). The used stack-up including four layers (a 0.25 mm-thick RO3010 substrate, a 1.0 mm-thick polystyrol layer, 5 mm of air, a 0.5 mm-thick RO4003 substrate) is displayed in Fig. 1.
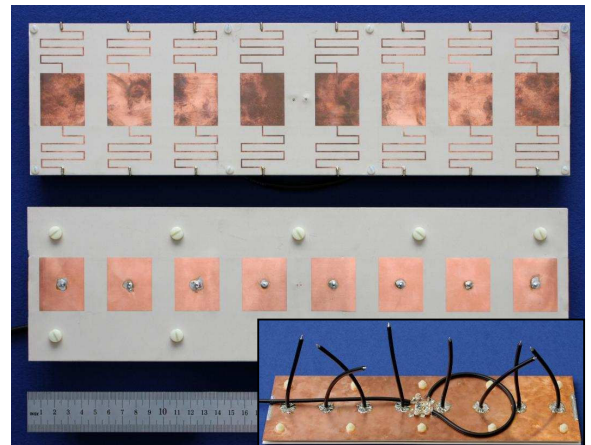

Fig. 6. Front- and back-side of the eight-cell MIM/coax-stubs prototype (bottom) together with an older prototype with meandered sidewise stubs, which has a larger transversal dimension (top).

[5]The part of the substrate without metal of the new cell must be cut away in order to be really narrower than the older cell with meandered stubs.

Finally the excited near-fields of the prototype inside a flat phantom (2 cm away from its lower bound) have been measured with probes from SPEAG (Zurich, Switzerland) – one for the magnetic field amplitude and another one for the SAR distribution. Our near-field measurement setup is shown in Fig. 7.
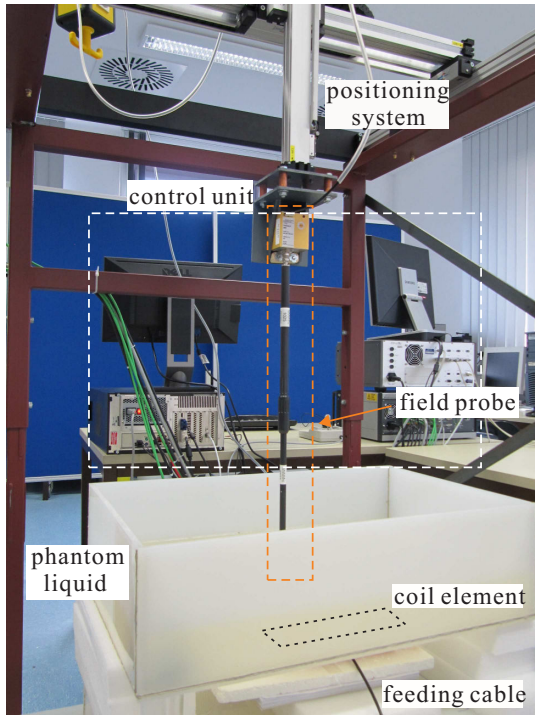

Fig. 7. Near-field measurement system comprising SPEAG's near-field probe, a positioner with three linear axes and a tank with the phantom liquid modelling the human body at 300 MHz.

The results are given in Fig. 8. The agreement between FDTD-simulation (cf. Fig. 5) and measurement for the near-field distributions is very good. A CW power of 20 W has been used for feeding the prototype, and the corresponding maximally measured values are $|\vec{B}_1|_{max} = 1.36\ \mu$T and $SAR_{max} = 3.42$ W/kg, respectively.

IV. CONCLUSION

A MIM/coaxial-stub CRLH TL structure has been proposed. Its development was driven by a 7-Tesla MRI application. The novel CRLH topology exhibits advantages, especially for this near-field application, such as transversal compactness, polarization purity and field distribution. These advantages are due to a novel realization of the shunt inductor by using a short-circuited coaxial cable. The usage of the RF coil element is very flexible in terms of the size of the field-of-view. Due to the zeroth-order operation the longitudinal coverage can be ajusted in a very simple manner by changing the number of unit cells, and due to the narrow width of the element the azimutal coverage can be ajusted by a proper choice of the no of elements of the multi-channel setup, e.g., a four-channel setup for wrist- or knee-imaging and a 16-element arrangement for whole-body MRI.

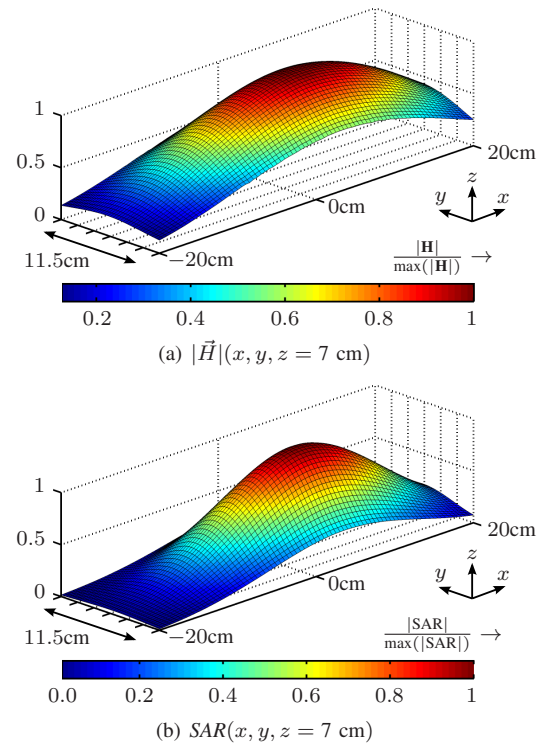(a) $|\vec{H}|(x, y, z = 7$ cm$)$

(b) $SAR(x, y, z = 7$ cm$)$

Fig. 8. Measured near-fields 2 cm inside the flat phantom.

In the future we will investigate the coupling performance of adjacent elements and we will evaluate the RF element in the MRI scanner, firstly by using phantoms.

REFERENCES

[1] C. Caloz and T. Itoh, *Electromagnetic Metamaterials, Transmission Line Theory and Microwave Applications.* Wiley and IEEE Press, 2005.
[2] C. Caloz, T. Itoh, and A. Rennings, "CRLH metamaterial leaky-wave and resonant antennas," *IEEE Antennas Propagat. Magazine*, vol. 50, no. 5, pp. 25-39, Oct. 2008.
[3] R. H. Hashemi, W. G. Bradely, and C. J. Lisanti, *MRI - The Basics.* Lippincott Williams & Wilkins, 2004.
[4] A. Rennings, J. Mosig, A. Bahr, C. Caloz, M. E. Ladd, and D. Erni, "A CRLH metamaterial based RF coil element for magnetic resonance imaging at 7 Tesla," in Proc. *3rd European Conference on Antennas and Propagation (EuCAP 2009)*, March 23-27, Berlin, Germany, Session Thu-P-4.57, pp. 3231-3234, 2009.
[5] J. Mosig, A. Bahr, T. Bolz, A. Bitz, S. Orzada, "Detailed investigations of a metamaterial transmit/receive coil element for 7 T MRI," in Proc. *Intl. Soc. Mag. Reson. Med. 18* (2010), #3856.
[6] A. Senn, A. Peter, and J. G. Korvink, "An 8-Channel metamaterial T-R coil at 9.4T," in Proc. *Intl. Soc. Mag. Reson. Med. 19* (2011), #1817.
[7] S. Otto, A. Rennings, K. Solbach, and C. Caloz, "Complex frequency versus complex propagation constant modeling and Q-balancing in periodic structures," in Proc. *IEEE MTT-S Int. Microwave Symp. (IMS2012)*, June 17-22, Montral, Canada, Session WEPL-1, 2012.
[8] S. Otto, A. Rennings, K. Solbach, and C. Caloz, "Transmission line modelling and asymptotic formulas for periodic leaky-wave antennas scanning through broadside," *IEEE Trans. Antennas Propagat.*, vol. 59, no. 10, pp. 3695-3709, Oct. 2011.